



CHORUS

This is the accepted manuscript made available via CHORUS. The article has been published as:

Ultracold Electron Bunch Generation via Plasma Photocathode Emission and Acceleration in a Beam-Driven Plasma Blowout

B. Hidding, G. Pretzler, J. B. Rosenzweig, T. Königstein, D. Schiller, and D. L. Bruhwiler

Phys. Rev. Lett. **108**, 035001 — Published 17 January 2012

DOI: [10.1103/PhysRevLett.108.035001](https://doi.org/10.1103/PhysRevLett.108.035001)

Ultracold Electron Bunch Generation via Plasma Photocathode Emission and Acceleration in a Beam-Driven Plasma Blowout

B. Hidding,^{1,2} G. Pretzler,² J. B. Rosenzweig,¹ T. Königstein,² D. Schiller,¹ and D. L. Bruhwiler³

¹*Department of Physics and Astronomy, University of California Los Angeles, USA*

²*Institut für Laser- und Plasmaphysik, Heinrich-Heine-Universität Düsseldorf, 40225 Düsseldorf, Germany*

³*Tech-X Corporation, Boulder, USA*

(Dated: November 23, 2011)

Beam-driven plasma wakefield acceleration using low-ionization-threshold gas such as Li is combined with laser-controlled electron injection via ionization of high-ionization-threshold gas such as He. The He electrons are released with low transverse momentum in the focus of the co-propagating, non-relativistic-intensity laser pulse directly inside the accelerating/focusing phase of the Li blowout. This concept paves the way for generation of sub- μm -size, ultralow-emittance, highly tunable electron bunches, thus enabling a flexible new class of advanced FEL-capable high-field accelerator.

PACS numbers: 52.38.Kd, 41.75.Jv, 52.35.Mw

One of the most attractive aspects of plasma-based accelerator schemes is that electric fields of tens of GV/m or more can be generated for acceleration. Such fields are orders of magnitude higher than in classical metallic cavity-based accelerator structures (~ 100 MV/m) or in recently considered dielectric waveguide structures (~ 1 GV/m) [1]. Driven in the most promising configuration by either a powerful laser pulse [2, 3] or a high charge electron beam [4], nonlinear plasma waves can be induced which are fully cavitated. This disturbance produces longitudinal electromagnetic wakes ideal for acceleration, as well as linear focusing of beam electrons due to the ion column in the electron-rarefied cavity where the acceleration optimally takes place. The plasma cavity length is similar to the plasma wavelength $\lambda_p \propto n_e^{-1/2}$ and thus may be tuned by changing the ambient plasma electron density n_e . Further, the accelerating field amplitude is also related to n_e as $E_z \propto n_e$. These dependences dictate that if >10 GV/m-scale fields are desired, one requires an n_e that corresponds to few 10's of μm -scale accelerating structures. This scenario presents serious experimental challenges in beam generation, and in controlling the accelerated beam quality. Nevertheless, remarkable progress has been made in recent years [5, 6], and various techniques for ameliorating and managing the injected beam characteristics have been demonstrated. Injection of electrons into the transient plasma electron blowout is of paramount importance, since it defines the initial phase space volume and position within the blowout. External injection of beams generated by a conventional device is possible [7], but it is also very attractive to inject electrons from the plasma itself, thus combining the electron source with the main accelerator section. A multitude of injection techniques with laser-plasma accelerators have been developed and demonstrated, such as colliding pulse injection [8–11], ionization-induced injection [12–16], and plasma density transition injection [17–21].

Here we present a fundamentally new scheme in which

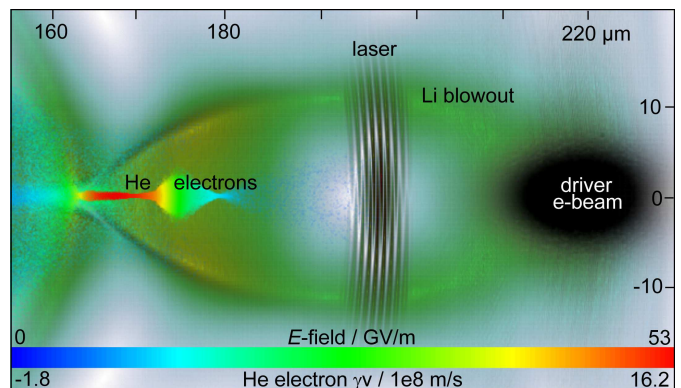


FIG. 1. Results from a VORPAL [25] simulation show how an electron driver ionizes Li gas and generates a Li blowout with an electron density of $n_e(\text{Li}) = 3.3 \times 10^{17} \text{ cm}^{-3}$, corresponding to a linear plasma wavelength of $\lambda_p(\text{Li}) \approx 60 \mu\text{m}$. The Ti:Sa laser pulse with a duration of $\tau \approx 8$ fs and $a_0 = 0.018$ is located at the end of the first half of the blowout at the electric field's turning point, and has already ionized some He electrons, which are then trapped and accelerated.

it is possible to release electrons directly into the accelerating and focusing phase of relativistic beam-driven plasma cavities, which may enable dramatically reduced bunch dimensions and emittance. Consider first an electron beam-driven plasma wakefield acceleration (PWFA) scenario. State-of-the-art electron beams today may have self-fields which are high enough to ionize low-ionization threshold gases such as Li, thus even making it possible to use beam-ionized instead of preionized plasma. Such electron beams can either be produced in standard [22] or in laser wakefield accelerators (LWFA) [23]. The ongoing worldwide increase of LWFA facilities capable to generate ultradense electron bunches, accompanied with improvement of LWFA beam quality, leading to fs-scale lengths and energy spreads down to the $< 1\%$ [24] level, makes these bunches good candidates as PWFA drivers.

The accelerating and focusing phase of the plasma

blowout has ideal characteristics for the acceleration of electrons [4]. In order to inject electrons directly into this phase, we propose to use even comparably low-power, high repetition rate, kHz-type laser pulses with fs-scale duration τ , that can have focused intensities and corresponding electric fields which are orders of magnitude higher than the electric fields of even the most intense electron bunches available today. Using the normalized wave vector potential a_0 , the amplitude of these fields is expressed as $E_0 = a_0 2\pi m_e c^2 / (e\lambda)$, where λ is the laser pulse wavelength. A Ti:Sa laser ($\lambda = 800$ nm) pulse with $a_0 = 0.018$, corresponding to a modest intensity of $I \approx 7 \times 10^{14}$ W cm $^{-2}$, has focal electric fields up to $E_0 \approx 72$ GV/m, high enough to ionize a high-ionization threshold gas such as helium. In a mixture of Li and He gas, the driving electron beam self-fields can be adjusted to ionize only the Li component, while the He would remain neutral despite the passage of the electron driver. In contrast, the properly timed laser pulse can easily ionize the He fraction, thus giving rise to He electrons at an arbitrary position within the Li blowout.

Figure 1 shows fully explicit 2D cartesian particle-in-cell simulation results obtained with the parallel VORPAL framework [25]. The moving window simulation box size was $110 \times \lambda$ in longitudinal direction with a cell length down to $\lambda/16$ in order to resolve the laser wavelength λ , and in transverse direction $110 \times \lambda$ at a cell width down to $\lambda/8$ to resolve the witness bunch width. The simulation uses 3rd order particle shapes and ADK tunneling ionization.

The driver electron beam (driver density is color coded black/white) has transverse and longitudinal dimensions $\sigma_r = 5 \mu\text{m}$, $\sigma_z = 7 \mu\text{m}$ RMS, a charge of $Q \approx 300$ pC at an energy of $W = 200$ MeV, with a notable energy spread of $\Delta W = 10\%$. Such a beam has a transverse electric field of $E_r(r) = Q / [(2\pi)^{3/2} \sigma_z \epsilon_0 r] [1 - \exp(-r^2 / (2\sigma_r^2))]$, peaking at $E_{r,\text{max}} \approx 27$ GV/m. This is enough to field-ionize Li effectively, while not sufficient to liberate He electrons by the same mechanism [26]. With a maximal Li electron density of $n_e(\text{Li}) = 3.3 \times 10^{17}$ cm $^{-3}$ and a beam density $n_b = Q / [(2\pi)^{3/2} e \sigma_r^2 \sigma_z] \approx 6.6 \times 10^{17}$ cm $^{-3}$, a moderate blowout is driven with a plasma wavelength of $\lambda_p(\text{Li}) \approx 60 \mu\text{m}$. The maximum accelerating field observed in the simulation reaches $E_z \approx 50$ GV/m, near to the classical wave breaking limit $E_{\text{WB}} = 2\pi m_e c^2 / (e\lambda_p)$. Here, the electric field magnitude is plotted, rendering visible not only the blowout, but also the laser pulse which is linearly polarized in the simulation plane.

The laser pulse moves collinearly with the driver beam (in an experimental scenario, focused by a flat or parabolic mirror with a hole created for drive beam passage), with a focal (vacuum) waist of $w_0 = 4 \mu\text{m}$ at a longitudinal coordinate of $z = 132 \mu\text{m}$. Here, both the Li and He gas density reach a flat maximum, after having been ramped up linearly. In Figure 1, the laser pulse has already passed its focal point, is defocusing and

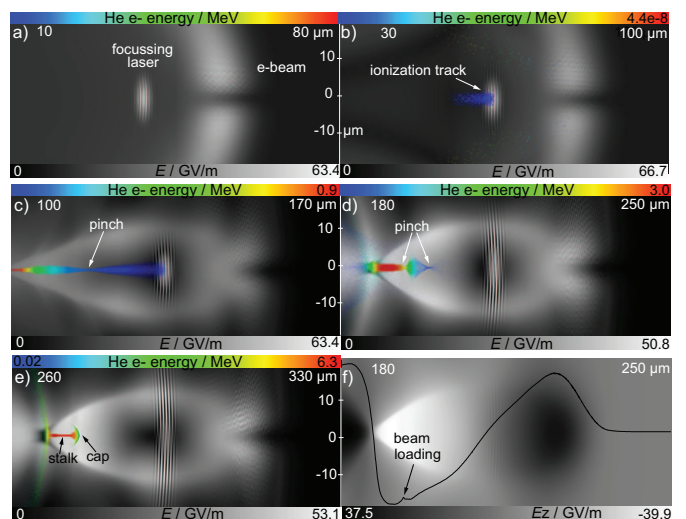


FIG. 2. Injection of He electrons at the beginning of the interaction. Snapshots a) to e) show E generated by the Li blowout and the laser pulse, and the He electrons which are born inside the Li blowout due to ionization by the focussed laser pulse, while f) shows only E_z and a line out on axis, corresponding to d).

its intensity has just dropped below the He ionization threshold. The He electrons which have been previously released by ionization are plotted with color coded energy. A large fraction of the He electrons has already gained relativistic longitudinal momentum $p_z/m_0 = \gamma v_z$ and therefore is trapped, travelling with sufficient velocity to remain in the PWFA cavity. As a result of an interplay between upramping Li and He gas densities $n_e(\text{Li})$ and $n_e(\text{He})$ (and therefore a decreasing plasma wavelength $\lambda_p(\text{Li})$, leading to contracting Li blowout region), the relative position of released He electrons within the Li blowout, and their integrated acceleration history $\int dE_z dz$ varies. This is reflected by varying longitudinal normalized He electron momenta, ranging from $p_z/m_0 = \gamma v_z \approx 16.2 \times 10^8$ m/s down to a few counter-propagating electrons $\gamma v_z \approx -1.8 \times 10^8$ m/s. The simultaneous effects of the electron momentum distribution, relative position and collective radial electric field exerted by the Li blowout electrons are responsible for the double-pinch He electron beam structure in the snapshot.

Figure 2 illustrates the injection and trapping process in more detail via snapshots of the field magnitude E and the He electron macroparticles and energy in the longitudinal direction as a result of the Li based wake-field driven by the electron beam. In Figure 2 a), the laser pulse is converging, not yet having reached its focal point $z = 132 \mu\text{m}$, and is not yet intense enough to initiate ionization. But as seen in 2 b), after $< 20 \mu\text{m}$ further propagation, the electric field amplitude has gained another 3 GV/m, enough to ionize He and leave behind electrons near-axis. In snapshot 2 c), the laser

pulse has traveled past its focus slightly, and therefore again has marginally lost its ability to ionize He. The Li blowout here is not fully closed yet due to the gas density up-ramp. Pinching of the He electrons has evolved dynamically, and the blowout begins closing behind the electrons that have been injected by the laser-induced ionization (see Figure 2 d). At this point, the Li-electron-based cavity has reached its steady-state length of $\lambda_p(\text{Li}) \approx 60 \mu\text{m}$, corresponding to the maximum electron density of $n_e(\text{Li}) = 3.3 \times 10^{17} \text{cm}^{-3}$ at the end of the density up-ramp. The electrons trapped inside the cavity are now co-moving with the driver and have reached a significant energy ($W_{z,\text{max}} \approx 3 \text{MeV}$). During the further acceleration process (see Figure 2 e), a mushroom-like structure evolves, the highest energy electrons forming the stalk, and lower-energy (but still relativistic) electrons forming the cap. Note that the laser pulse is still clearly visible in the electric field magnitude plot, but does not notably affect the Li electron blowout. In Figure 2 f), the longitudinal electric field E_z contribution to the total electric field in 2 d) is plotted along with an on-axis line-out, which reveals that the injected He electrons significantly distort the electric field due to beam loading (self-wake) and space charge.

With the initial phase of the injection/acceleration process concluded, the beam-driven PWFA process continues to provide acceleration, in principle limited only by the total energy of the driver and/or its density distribution. Our simulations confirm that the acceleration can continue for long distances without degrading the He electron bunch quality. Figure 3 a) illustrates the situation after $z = 2.5 \text{mm}$. While the driver electron beam (not plotted) and the electric field generated by it show scalloping as in ref. [6], the He electrons remain confined on axis, and form a bunch with FWHM widths of only a few hundred nm or less. In Figure 3 a), the FWHM width amounts to $\sigma_{r,\text{He}} \approx 150 \text{nm}$. In this sense, the proposed acceleration concept can be seen as a bunch width transformer: when compared to the driving beam, the accelerated He electron beam has a width which is smaller by more than an order of magnitude. This is a result of the He electrons a) being born close to the axis, and b) receiving low transverse momentum by the low-power laser. A divergence of $\approx 1.13 \text{mrad}$ at an energy of $W \approx 108 \text{MeV}$ leads to a calculated normalized transverse slice emittance on the central $5 \mu\text{m}$ long bunch section (the position indicated in the figure with the black arrows), of $\epsilon_n \approx 3 \times 10^{-8} \text{mrad}$, which is observed to increase to $\epsilon_n \approx 4 \times 10^{-8} \text{mrad}$ until the bunch has reached the same γ as the wake. Such an excellent normalized emittance, which is one or two orders of magnitude better than with any previous scheme, is in agreement with considerations centered on the laser vector potential. For a laser with $a_0 \approx 0.018$, the expected minimal emittance (assuming the initial transverse beam source size $\sigma_{r,\text{He}}$ generated by the laser is $\sigma_{r,\text{He}} \approx w_0/\sqrt{2}$,

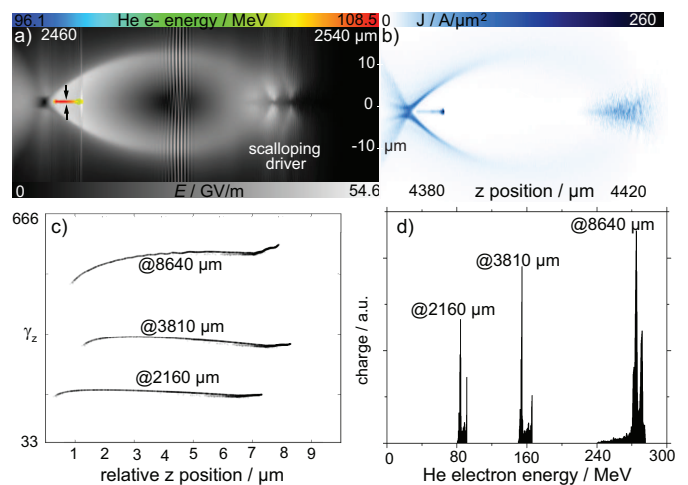


FIG. 3. Electric field and He bunch after $z = 2.5 \text{mm}$ (a), current J after $z = 4.4 \text{mm}$ (b), $p_z - z$ phase space for three different acceleration times (c), and He electron energy spectrum at these times (d).

and using $\sigma_{p_r}/(mc) \approx a_0/2$) can be estimated to be $\epsilon_n \approx \sigma_{r,\text{He}}\sigma_{p_r}/(mc) \approx w_0 a_0/2^{3/2} \approx 2.6 \times 10^{-8} \text{mrad}$. This is one of the critical advantages of the acceleration scheme, which opens up the possibility of its use in future advanced FEL-based X-ray light sources, where emittance has a limiting effect on performance and reachable wavelength. For example, an approximation for the minimum wavelength based on the above emittance and an energy similar as in the Linac Coherent Light Source (LCLS) results in $\lambda_{\text{min}} \approx 4\pi\epsilon_n/\gamma_{\text{LCLS}} \approx 0.1 \text{\AA}$, about one order of magnitude better than the current LCLS performance [27]. We have also performed GENESIS simulations of the case in which the beam presented here is accelerated up to 4.3GeV , and used with a next generation undulator [28]; this scenario promises a 1.5\AA SASE FEL that saturates in $\sim 20 \text{m}$, a dramatically shorter distance than the LCLS.

Figure 3 b) shows the current density which is calculated after about $z \approx 4.4 \text{mm}$, and reaches peak values of $J \approx 260 \text{A}/\mu\text{m}^2$. With a total charge of $Q \approx 2 \text{pC}$, a peak bunch current can be approximated to be $I_p \approx 300 \text{A}$, which leads to a brightness of $B \approx 2I_p/\epsilon_n^2 \approx 7 \times 10^{17} \text{Am}^{-2}\text{rad}^{-2}$, again a value one or two orders of magnitude better than with the LCLS. In Figure 3 c) and d), the longitudinal phase space and the energy spectra of the transversally ultracold He electron bunch are depicted at three different points during acceleration. For the chosen parameters, the He-derived electrons reach a peak energy of nearly $E \approx 300 \text{MeV}$ after about $z \approx 9 \text{mm}$ of acceleration, with an energy spread $\Delta W \approx 3\%$. It shall be noted that the acceleration length, and thus the peak He electron bunch energy is mainly limited by the driver energy and its degradation. Keeping the density in the range $\sim 10^{17} \text{cm}^{-3}$ and raising the driver beam

energy to multi-GeV level (such as the SLAC beam) will enable maintaining the blowout without quality degradation over meter-long distance, reaching GeV-scale energies.

In summary, we have conceived and presented a new, promising ionization-based injection and acceleration scheme in the context of the PWFA, which is characterized by direct, low transverse momentum deposition of electrons directly inside the accelerating and focusing phase of a plasma blowout cavity. Essential components are the use of two gas species with substantially different ionization thresholds (or a single species with substantially different ionization thresholds such as Cs), and driver electron beams which are able to ionize the low-ionization-threshold gas component in order to set up the driver blowout. Since the electrons to be accelerated are planted in a highly-controlled way, making use of a moderate intensity, non-relativistic laser pulse just above the ionization threshold of the second gas component, electron beam distribution shaping is possible, and ultralow emittance and high current/high brightness beams can be produced. This possibility may have far-reaching consequences for example for future FEL schemes based on this concept, potentially enabling sub-angstrom wavelengths and improved brightness.

The confidence level in the experimental feasibility of the described scheme is high. Previous PWFA experiments at SLAC in He-confined Li ovens have already demonstrated the possibility of He ionization (in this case, caused rather uncontrolled by density oscillations of the driver electron beam), injection and He electron acceleration up to many GeV [29] – an experimental scenario similar to what would be needed for a proof-of-concept experiment. Future PWFA setups, which might use Cs or Rb instead of Li due to reduced head erosion, are also excellently suited for cold plasma photocathode release and acceleration. The second ionization level of Cs (25.1 eV) or Rb (27.3 eV) would then be used by the laser to release electrons instead/in addition to the first ionization level of helium (24.6 eV). It shall be noted that while the presented simulations are based on beam-driven ionization, pre-ionization of the low-ionization threshold component is an attractive option, too. The ionization potential I_p difference between the first ionization threshold of Li, Rb, or Cs and the second ionization threshold of Rb or Cs or the first ionization threshold of helium, respectively, is more than 20 eV. Since the laser intensity required for ionization scales even stronger than linearly (in case of Barrier Suppression Ionization, $I_{th} \propto I_p^4$), laser-based pre-ionization of the low-ionization threshold component without ionizing the high-ionization threshold component is feasible, and can lead to enhanced acceleration lengths and a higher stability of the scheme.

LWFA facilities have the potential to produce all-optical versions of the presented scheme, where the main laser pulse would be used to produce the higher

charge, lower phase space quality electron beam driver, and a small, inherently synchronized split-off laser pulse would be subsequently used for electron release into the blowout. Synchronization of a laser pulse with conventional electron beam drivers is more difficult, but for example at LCLS, where pump-probe experiments are essential, sub-100-fs jitters have been already reported. The presented concept is robust to spatial (laser pointing) and temporal (laser timing) fluctuations. The supplemental material shows that, for example, injection, trapping and acceleration still takes place when the laser pulse has a delay of ± 43 fs when compared to the above presented example case. When the laser pulse is off axis (by 1 and 3 μm , respectively), injection and acceleration works, too. In that cases, very distinct betatron oscillations occur (see Supplemental Material), which could be exploited directly for xray generation.

We acknowledge fruitful discussions with P. Muggli. This work was supported by the German Research Foundation DFG TR 18, by the US Department of Energy DOE under contracts No. DE-FG02-07ER46272 and DE-FG03-92ER40693, and by the Office of Naval Research ONR under contract No. N00014-06-1-0925. BH thanks DAAD for support. DLB was supported by Tech-X Corp., and by DOE grant No. DE-FC02-07ER41499 and acknowledges the assistance of the VORPAL development team. This research used resources of the National Energy Research Scientific Computing Center, which is supported by DOE grant DE-AC02-05CH11231.

-
- [1] M. C. Thompson *et al.*, Phys. Rev. Lett. **100**, 214801 (2008).
- [2] T. Tajima and J. M. Dawson, Phys. Rev. Letters **43**, 267 (1979).
- [3] A. Pukhov and J. Meyer-ter Vehn, Applied Physics B-Lasers and Optics **74**, 355 (2002).
- [4] J. B. Rosenzweig *et al.*, Phys. Rev. A **44**, R6189 (1991).
- [5] W. P. Leemans *et al.*, Nature Physics **2**, 696 (2006).
- [6] I. Blumenfeld *et al.*, Nature **445**, 741 (2007).
- [7] C. E. Clayton *et al.*, Phys. Rev. Lett. **70**, 37 (1993).
- [8] D. Umstadter *et al.*, Phys. Rev. Lett. **76**, 2073 (1996).
- [9] E. Esarey *et al.*, Phys. Rev. Lett. **79**, 2682 (1997).
- [10] J. Faure *et al.*, Nature **444**, 737 (2006).
- [11] X. Davoine *et al.*, Phys. Rev. Lett. **102**, 065001 (2009).
- [12] M. Chen *et al.*, Journal of Applied Physics **99**, 056109 (2006).
- [13] C. McGuffey *et al.*, Phys. Rev. Lett. **104**, 025004 (2010).
- [14] C. E. Clayton *et al.*, Phys. Rev. Lett. **105**, 105003 (2010).
- [15] B. B. Pollock *et al.*, Phys. Rev. Lett. **107**, 045001 (2011).
- [16] J. S. Liu *et al.*, Phys. Rev. Lett. **107**, 035001 (2011).
- [17] H. Suk *et al.*, Phys. Rev. Lett. **86**, 1011 (2001).
- [18] C. G. R. Geddes *et al.*, Phys. Rev. Lett. **100**, 215004 (2008).
- [19] K. Schmid *et al.*, Phys. Rev. ST AB **13**, 091301 (2010).
- [20] S. Y. Kalmykov *et al.*, Plasma Physics and Controlled Fusion **53**, 014006 (2011).
- [21] A. J. Gonsalves *et al.*, Nat Phys **7**, 862 (2011).
- [22] J. Rosenzweig *et al.*, NIM A **653**, 98 (2011).
- [23] B. Hidding *et al.*, Phys. Rev. Lett. **104**, 195002 (2010).
- [24] S. M. Wiggins *et al.*, Plasma Physics and Controlled Fusion **52**, 124032 (2010).
- [25] C. Nieter and J. R. Cary, Journal of Computational Physics **196**, 448 (2004).
- [26] D. L. Bruhwiler *et al.*, Phys. Plasmas **10**, 2022 (2003).
- [27] B. W. J. McNeil and N. R. Thompson, Nat. Photon. **4**, 814 (2010).
- [28] F. H. O'Shea *et al.*, Phys. Rev. ST AB **13**, 070702 (2010).
- [29] E. Oz *et al.*, Phys. Rev. Lett. **98**, 084801 (2007).